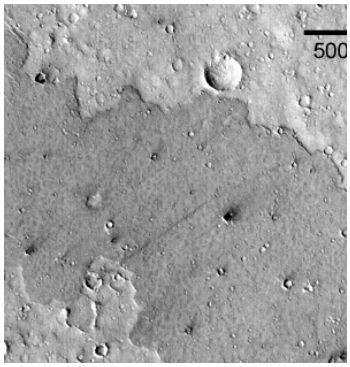


ISOCHRONS FOR MARTIAN CRATER POPULATIONS OF VARIOUS AGES

Text: William K. Hartmann

Page design & maintenance: Daniel C. Berman

Planetary Science Institute, Tucson



BACKGROUND B USING CRATER COUNTS TO ESTIMATE AGES

Below you will find a text describing the basic principles behind the Planetary Science Institute system of utilizing crater counts and isochron diagrams in order to estimate crater retention ages of surfaces on Mars.

As discussed by Hartmann (1966) the crater numbers can date the actual formation age of a surface in an ideal case, such as a broad lava flow which forms a one-time eruptive event. The flow accumulates craters and the crater numbers date the time of formation. In other cases, not uncommon on Mars, the story is more complex. For example a surface may be covered by a few hundred meters of mobile sand dunes; the numbers of craters of diameter D and depth d would give a mean characteristic age of topographic features of the scale of D,d. Smaller craters in mobile dunes would disappear faster and have lower mean ages. In this sense, the derived age is a size-dependent Acrater retention age@ B the survival time of craters of given size. It is not quite a formation age in the sense of the lava flow age, but conveys tremendous information about the erosion/deposition/resurfacing environment of Mars.

Another example is exhumation, which is common on Mars (Malin and Edgett 2000, 2001). A surface could be formed and covered by sediments at some later time, degrading any craters on the original surface. Much later, the surface may be exhumed, as documented in various cases by Malin and Edgett. In an ideal case, such a surface might then show vestiges of the degraded original craters (indicating the duration of exposure of the first surface) and a second population of fresh, small, sharp-rimmed craters formed since the recent exhumation event. Malin and Edgett (2001, 2003), thinking in terms of dating the underlying process, asserted that such processes render Martian crater counts more or less useless for dating. On the contrary, such a situation can give extremely valuable estimates of the timescale of the exhumation processes, not to mention the timescale of exposure of the original underlying surface (which in turn is a lower limit to its age). Indeed, Hartmann et al (2001) found just this situation in the Terra Meridiani hematite-rich area, which they identified as a very ancient surface recently exhumed within the last few tens of My, because of the paucity of small, sharp-rimmed, fresh craters -- an interpretation which appears consistent with observations from the 2004 Opportunity rover, which landed in this same general area on a sparsely cratered plain and found sulfate-rich sediments apparently eroding and leaving small, spherical hematite concretions which weathered out of the sediments as they eroded.

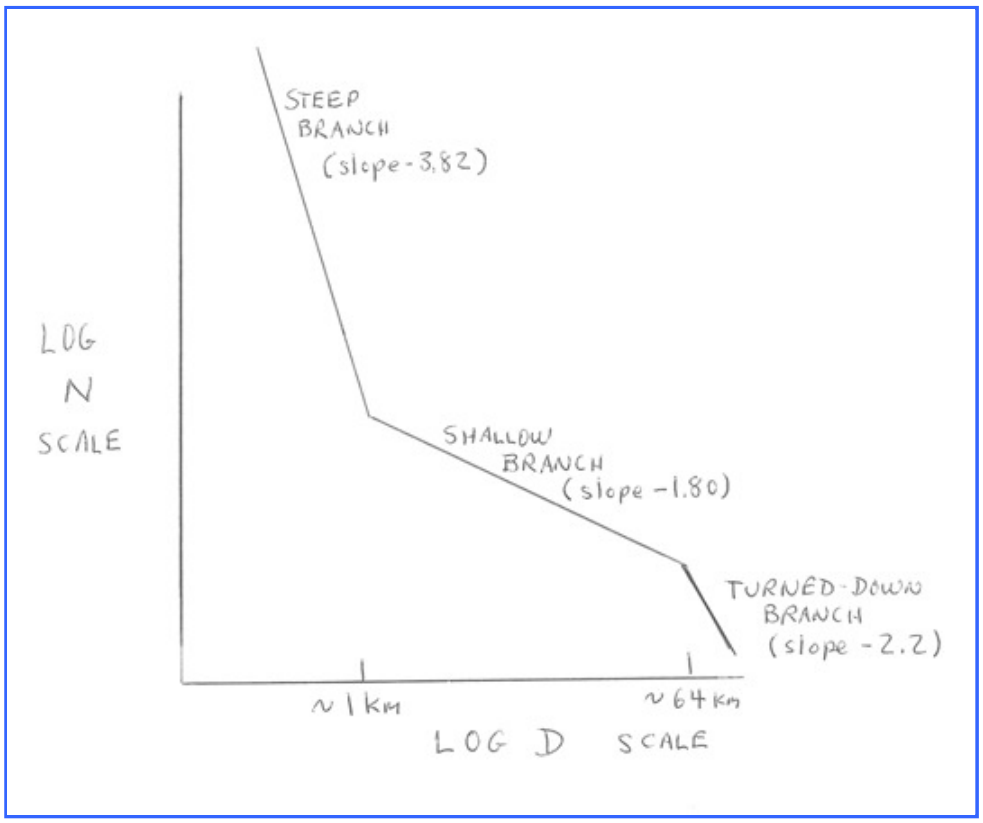
In general, however, in dating Martian units, we look for simpler situations where a relatively homogenous stratigraphic unit is identified, and which appears not to be contaminated by secondary-ejecta impact craters from any single, nearby, large fresh primary impact crater. We assume that in such a case, a gradual accumulation of primary impact craters and globally-averaged (or regionally-averaged) secondary ejecta craters will have built up a characteristic diameter distribution shape, sometimes called the “crater production function.” Usually we count all visible craters and test to see if the size distribution fits the so-called Acrater production function@ B the size distribution previously measured for accumulated primary and secondary impact craters, globally averaged in the absence of erosion/deposition processes. If so, we compare the measured size distribution to the Aisochrons@ derived below. An isochron is defined as a size distribution of all craters created, as described above, over a specified period of years, such as 100 My or 1 Gy.

INTRODUCTION TO THE SIZE DISTRIBUTION B SHALLOW BRANCH, STEEP BRANCH, AND TURNED-DOWN

The diagram we use to plot craters combines ease of use, maximum sensitivity to possible crater losses at particular sizes, and mathematical convenience (since, by mathematical coincidence, it has the same slope as a plot of

cumulative number of craters vs. D). This diagram divides the D range into log intervals with base /2. For example, bin divisions include 500 m, 707 m, 1 km, 1.4 km, 2 km, 2.8 km, and so on. The vertical axis gives N = no. craters/km^2 in each bin, and the horizontal axis gives D, divided as indicated above. The diagram is essentially a histogram, plotting the number of craters/km^2 in each of these log-D bins.

Figure 1 gives a schematic representation of the shape of a well-preserved, or Aproduction,@ size distribution on this type of plot. In the text below, we will refer to three Abranches@ of this size distribution. Historically, the first branch recognized was the shallow branch, at diameters above about 1-2 km, recognized from craters counted on telescopic photos of the moon. (See historical review by Hartmann, 2004, submitted to Icarus). This has been identified with the mix of asteroidal and cometary interplanetary fragments, and such craters are called Aprimary@ craters, connoting that they originate from cosmic debris falling from the sky at high speed. The first papers on diameter distributions of craters, meteoroids, and asteroids, fitted those distributions to power laws of the form N = k D^{-b} and typically found b ~ -2 for lunar craters. The b value also equals the slope on our plot or on a cumulative plot. A more comprehensive study by the Basaltic Volcanism Study Project in 1981 give a least squares fit slope of -1.8 for lunar craters in this branch (Hartmann et al. 1981).



[Fig. 1]

The second branch to be recognized was the steep branch, at D < ~1 km, first seen in 1964 when the Ranger probes gave the first sub-km resolution views of the moon. Shoemaker (1965) showed that secondary impact craters caused by ejecta from large lunar craters such as Copernicus, Langrenus, etc, fit this steep slope, and Shoemaker hypothesized that the small lunar craters in this branch are completely dominated by secondary ejecta from lunar craters. Hartmann (1969) showed from empirical data that fragments from low-energy-density disruption events (and craters made by them) are associated with the lower slope, while fragments from high-energy-density environments (such as hypervelocity impact crater transient cavities) associate with the higher slope, fitting this view. Hartmann and Gaskell (1997, p. 113) found a representative slope of -3.82 for this branch in the D interval viisible in lunar maria, about 1 km down to about 250 m, although further work is needed to understand the extent of local variations (if any) in the slope of the steep branch.

Strom, Neukum, and others eventually concluded that at the largest diameters, above 64 or even 100 km, the curve has a Aturned down branch.@

At this point, Neukum (1983) made the reasonable decision to abandon the concept of multiple power law segments and simply fit the curve to a polynomial function. He developed a function which he has found to fit production-function craters on the moon, Mars, and asteroids (with appropriate scaling considerations).

Neukum and Ivanov (1994) challenged the Shoemaker-era conclusion and terminology, that the steep branch on the moon (or Mars) is associated with secondary ejecta from lunar (or Martian) primary craters. They found that the then-new high-resolution images of asteroids show a steep branch among sub-kilometer asteroidal craters B proving that the steep branch exists in space in the asteroid belt, suggesting in turn that even the Aprimary@ or cosmic impact craters on the moon and Mars, at these sizes, manifest the steep branch. In other words, they concluded that Shoemaker was not necessarily correct in assigning most sub-kilometer small craters to secondary impacts; they refer to the small craters as mostly Aprimaries@ in the sense that they could be cosmic. Hartmann (1999___) pointed out that this revision is somewhat semantic, because the steep branch found in the asteroid belt is presumably due to secondary ejecta from craters on asteroids B except that the pieces do not fall back onto the target asteroids but rather float in the belt and hit other asteroids. Thus, if the slope of the steep branch is controlled by crater ejecta (on one body or another) and if the crater ejecta size distributions are controlled by the mechanics of fragmentation in hypervelocity rock targets, the resultant slopes among lunar ejecta fallback, Martian ejecta fallback, and interplanetary asteroid ejecta may be negligible. Which is one reason that the size distributions among secondaries on in different environments deserve more investigation.

SIDEBAR: COMMENT ON OTHER TYPES OF PLOTS

This type of plot is called a log-differential plot It is better than the commonly-used cumulative plot of all craters larger than D, because it much more clearly shows losses of craters in any particular size bin. For example, if a certain region has had some erosive episode that removed all craters between 125 m and 500 m in size, the log-differential plot would show a dramatic downturn in that size interval, but he cumulative plot would merely flatten out. The cumulative plot produces an artificial smoothing of the data, which looks good, but comes at the expense of actual information-display about the data.

The log-differential plot is also more direct than a commonly-used type of plot introduced some years ago, called the Arelative plot@ or R-plot. This plots crater counts relative to an artificial -2 power law distribution ($N = kD^{-2)}$. It was introduced when the counters were dealing primarily with craters larger than 1 km, which roughly fit a -2 power law (more accurately, it is a -1.80 power law). Departures from the -2 power law were regarded as diagnostic. The problem is that we now count from D = 11 m up to multi-km sizes and the size distribution is much steeper at small sizes (power laws with slopes up to -3.____).

ESTABLISHING THE AMAZONIAN, HESPERIAN, AND NOACHIAN ERAS ON THE CRATER-COUNT DIAGRAM

Tanaka (1986, Table 2) defined crater density limits to the Amazonian, Hesperian, and Noachian relative-age eras, based on the previous work of Scott and Carr (1978) and Condit (1978), for the purpose of stratigraphic mapping of Mars. That work parallels the development of terrestrial geology, in defining stratigraphy and relative time intervals long before the absolute time intervals could be measured. Tanaka defined each time interval in terms of cumulative counts of craters down to various diameters *D*, namely 1 km for the Amazonian and Hesperian, and 5 for the Noachian. Note that, in those post Viking years, diameter distributions had not been studied much below $D = 1$ km. (Even the major review of Martian cratering studies in 1992 by Strom et al. did not include discussion of crater counts below diameters of a few km, although some Viking images resolved craters of a few hundred meters in size.) Upper *D* limits for the definitions were $D \sim 4$ km above the Amazonian/Hesperian boundary, and 16 km for early Hesperian to early Noachian. In these definitions, Tanaka assumed a -2 power law for the diameter distribution in that diameter range, an early approximation to the -1.80 power law used in that *D* range in our data. [Note: In the -2 approximation, our log-incremental count in a diameter bin (*D* to /2*D*) is equal to ½ the cumulative number given for all craters larger than *D*; for example, when Tanaka gives N = 160 craters/10^6 km^2 for $D > 1$ km for the late/mid Amazonian boundary, we give 8.00 (10^{-5}) craters/km^2 for the log incremental count of craters in the interval $1.0 < D < 1.41$ km (or, in Table 1, using Tanaka's -2 power law, 1.13 (10^{-4}) for the /2 log interval centered on $D = 1.0$ km)]. Applying these ideas and Tanaka's diameter intervals in our system, we calculate the following curves, defining the boundaries of the stratigraphic eras in our graphical system (note Tanaka, 1986, divided the Hesperian only into late and early subdivisions):

Late/mid Amazonian	log N (craters/km^2)	=	-2 log *D* (km) - 3.947 (1 km < *D* < 4 km)

Mid/early Amazonian	log N	=	-2 log *D* - 3.373 (1 km < *D* < 4 km)
Amazonian/Hesperian	log N	=	-2 log *D* - 2.947 (1 km < *D* < 4 km)
Late/early Hesperian	log N	=	-2 log *D* - 2.674 (1 km < *D* < 16 km)
Hesperian/Noachian	log N	=	-2 log *D* - 2.470 (1 km < *D* < 16 km)
Late/mid Noachian	log N	=	-2 log *D* - 1.742 (4 km < *D* < 16 km)
Mid/early Noachian	log N	=	-2 log *D* - 1.441 (4 km < *D* < 16 km)

These equations are used in Table 1 to calculate upper and lower endpoints of the diameter distribution segments used by Tanaka to define the eras, e.g., 1 to 4 km for the Amazonian/Hesperian boundary.

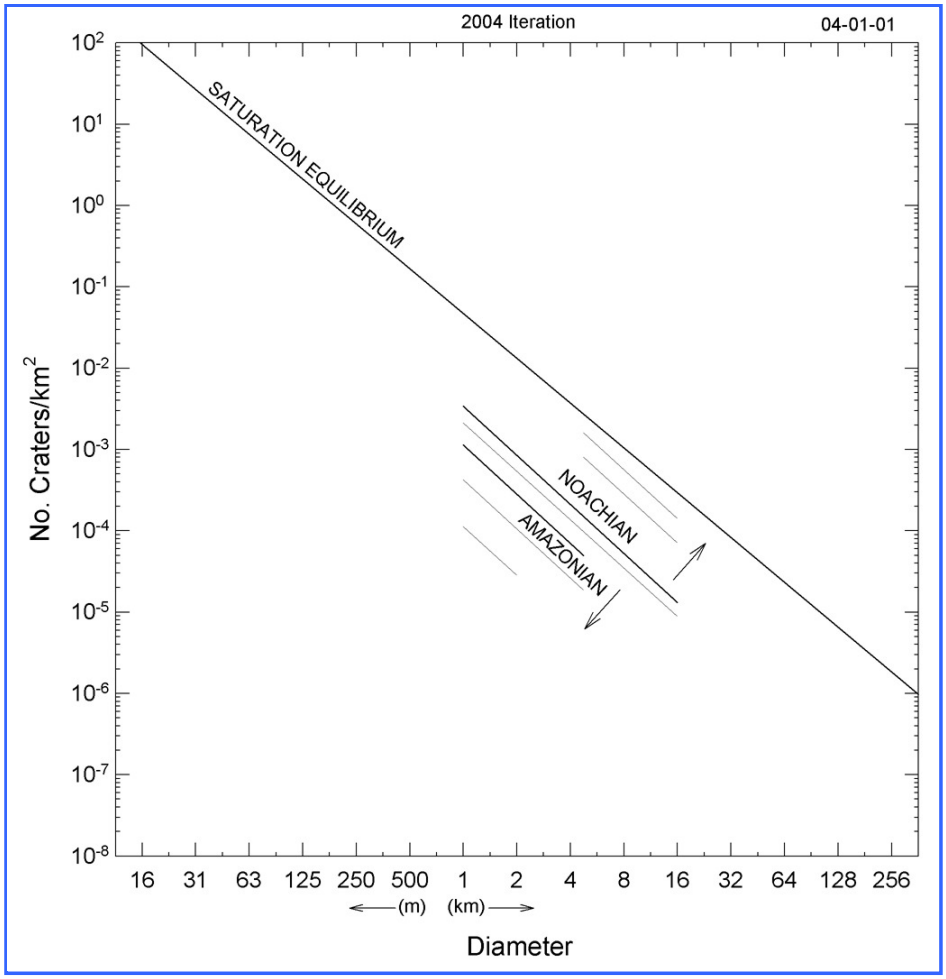
Table 1. End points for Amazonian/Hesperian/Noachian divisions

Division	*D* (km)	N	*D* (km)	N
Late/Middle Amazonian	1	1.130 (10^{-4})	4	7.061 (10^{-6})
Middle/Early Amazonian	1	4.236 "	4	2.648 (10^{-5})
Amazonian/Hesperian	1	1.130 (10^{-3})	4	7.061 "
Late/Early Hesperian	1	2.118 "	16	8.875 (10^{-6})
Hesperian/Noachian	1	3.388 "	16	1.324 (10^{-5})
Late/Middle Noachian	4	1.132 "	16	7.108 "
Middle/Early Noachian	4	2.264 "	16	1.415 (10^{-4})

Note: Upper and lower end points for each division correspond to maximum and minimum diameters for which Tanaka (1986) defined the system of Martian eras and subdivisions from crater counts. To be rigorous, the systems are undefined outside these endpoints. As explained in text, Tanaka assumed a power law exponent (or slope in our graphs) of -2, marginally different from the -1.80 value adopted here for most of these diameter intervals. *D* = diameter (km); N = craters/km^2 in $\sqrt{2}$ interval of *D*, evaluated at the *D* value listed.

[Table 1]

Figure 2 shows these curve segments, plotted in the format of the diagram we will use in presenting cratering data. The top solid line shows the level associated with saturation equilibrium of cratering, the maximum density that is reached. This was defined empirically for various solar system locations by Hartmann (1984) and tested experimentally by Hartmann and Gaskell (1977). Below this are shown the crater size distribution segments corresponding to Tanaka's definition of the eras. Figure 2 emphasizes that the fundamental definitions of Amazonian-Hesperian-Noachian chronology is tied to topography with 1 to 16 km scale. The diagram in this form, lacking isochrons, is good for relative dating relative ages in the U.S.G.S. stratigraphic system, but gives no information on absolute ages.



[Figure 2] Basic format of Mars crater count diagram. Upper dark, solid line, gives steady state saturation equilibrium crater density, as confirmed empirically and theoretically by Hartmann (1984) and Hartmann and Gaskell (1997). Heavy, short solid lines define boundaries of Amazonian, Hesperian, and Noachian, as defined in the diameter *D* intervals used by Tanaka (1986, Table 2). Short, lighter solid lines mark the subdivisions of the Noachian (early, middle, late), Hesperian (early, late – only two subdivisions were defined by Tanaka 1986), and Amazonian (early, middle, late), from the same source. This diagram is essentially a histogram, used to plot crater densities observed in each /2 *D* interval of crater diameter. We will derive isochrons showing number of craters/km^2 in each created in each *D* interval, for specified surface ages.

The Isochron System: Basic Steps and Historical Review

Our basic approach to deriving Martian surface ages has been developed in a multi-step process in the papers already cited. Here we update and expand the derivation in a six-step process listed below, with item (d) being a new addition in this paper, and several other items being updated:

(a) Assume that the size distribution and time dependence of impactor flux are the same on Mars as on the Moon (to first order), and start with the crater size distribution measured in the lunar maria (averaging over various lunar mare surfaces), with adopted average age 3.5 Ga. (This is consistent with the conclusion of Hiesinger et al., 2003, that, volumetrically, most lunar mare lavas date from 3.3 to 3.7 Ga ago; also, an average of ages of 20 lunar basaltic units, based on Apollo, Luna, and meteorite ages, gives 3.51 Ga (Stöffler and Ryder, 2001, Table V).

(b) Estimate the ratio R_{bolide} = ratio of meteoroids/km^3 at top of Mars atmosphere relative to the Moon, for any specified meteoroid size. The term "bolide," referring to luminous fireball phenomena in an atmosphere, is chosen to remind the reader that the R_{bolide} ratio is fixed only at the top of the atmosphere and that additional atmospheric losses must be taken into account. By (a), this ratio is assumed constant at all relevant sizes.

(c) Incorporate corrections for Mars/Moon crater diameter differences due to impact velocity and gravity scaling, and use these to...

(d) derive the size distribution expected on a hypothetical Martian surface of the same age as the average of the lunar

maria.

(e) Make corrections for the loss of the smallest meteoroids during meteoroid fragmentation in the Martian atmosphere.

(f) Using the assumed average age of lunar maria and time dependence assumption from step (a), ~ 3.5 Ga, use the measured relation of cratering vs. age (from the Moon) to derive Martian crater density for Martian surfaces of other ages.

This process gives a set of predicted "isochrons," or crater size-frequency distributions, for well-preserved surfaces of various ages, such as 1 Ga, 100 Ma, 10 Ma, and so on. The key is to think in terms of orders of magnitude; we want to distinguish 10^7 y surfaces from 10^8 y and 10^9 y surfaces in order to understand the gross planetary chronology. The system is not good enough to distinguish a 60 Ma lava flow from a 70 Ma flow, but that level of discrimination is less important at the current level of Martian scientific investigation.
Note again that we deal here with nearly the entire crater size spectrum. This contains more interpretive and chronological information than a simpler cumulative number of craters larger than some cutoff size, such as 2 km or 20 km, which is affected mainly by counts in the next two larger D bins. Also, the intervals used by Tanaka (1986) to define the Noachian, Hesperian, and Amazonian eras in terms of cumulative crater counts, namely 1 km < D < 16 km (see section 4 above) are useful in characterizing the gross "bedrock" geologic chronology, and establishing the overall Martian stratigraphy, but do not fully deal with the modification of old bedrock units by smaller-scale local obliterative processes, such as deposition of thin sediment layers, thin lava flows, and various sorts of erosion.
Consider that the Canadian shield has a basal age of the order 10^9 y, while the 10-m and 100-m-scale features have much lower ages due to glaciation, sedimentation, and other processes. Mars has this same nature, and the full diameter range of craters conveys much more information than a specific restricted diameter range. For example, the rim height of 1 km crater is about 35 m, and thus a succession of very young Amazonian flows totaling >35 m thick can cover craters of D < 1 km and reduce the observed mean crater retention age of a broader mid-Amazonian plain if measured at topographic scales of a < 1 km, without removing craters of D > 2 km. Observed sub-kilometer structure would all be Amazonian, while the underlying multi-km structures would be Noachian (similar to the example of the Canadian shield, above). A correct interpretation of the area would rely on features that could be found only in the full size spectrum – the older age from large craters and the young flows and their age from small-scale morphologies and the numbers of small craters. This situation is not uncommon on Mars.

Assumptions. To create isochrons for Mars, we make several assumptions that should be discussed further:

1) The size distribution of meteoroids hitting Mars is the same as that hitting the Moon (as mentioned in steps (a) and (b) above). We believe this should be true, since most dynamical effects are essentially size-independent. Meteoroid populations in the main belt in the size range .10 m and especially . 1 m may be significantly affected by the Yarkovsky and other effects, producing possible anomalies in both Martian and lunar crater diameter distributions below crater diameter D ~ 50 m and especially . 5 m, but this effect is probably similar on Mars and the Moon, and thus is minimized in the adoption of R_{bolide} (Farinella, et al., 1998; Hartmann et al., 1999).

2) The scaling corrections that will be used for impact velocity and gravity are diameter independent. A more detailed treatment might find a modest D dependence in these factors, but for our first-order discussion we assume that the Mars/Moon ratio of crater sizes formed by bolides of specified mass m is the same for all values of m.

3) The average impact rate ratio R_{bolide} between Mars and the Moon remains the same through time, if averaged over geological periods of time / 10 Ma. Individual asteroid breakup events could produce variations in the ratio over short time periods (fragment swarms on orbits that hit Mars and not Earth/Moon, or vice versa), but these should average out over periods longer than the dynamical half-life of fragments against ejection from the belt and collisions with planets (of the order 10^7 y), especially among the statistically more numerous smaller fragments.

Apropos assumption 3, the time dependence of the lunar cratering rate has been measured by several workers, and has been shown to be nearly constant within a factor ~ 2 averaged over the last 3000 Ma (Hartmann 1965, 1966b, 1970; Neukum, 1983; Grieve and Shoemaker, 1994; Neukum et al., 2001), so that crater densities are virtually proportional to age for ages younger than 3000 Ma. However, estimating the flux change in step (f) above, from the date of average lunar maria to 3000 Ma, introduces an uncertainty (as discussed by Hartmann and Neukum, 2001) estimated at a factor ~ 1.2 in either direction.
The greatest current uncertainty appears in step (b), in estimating R_{bolide}. This uncertainty is estimated as a factor ~

1.5 below. These two uncertainties are probably the greatest in the system. Hartmann (1999) conservatively estimated the total age uncertainty as a factor of 2 to 4 in either direction, larger at small $D < 100$ or 200 m.

This approach is different from that of Soderblom et al. (1974) and Neukum and Wise (1976), who based their methods on assumptions about the decline of cratering at the end of the era of early intense bombardment 3.9 Ga ago, rather than on explicit estimates of the Martian crater production rate. Also, this approach has gradually grown in sophistication. Hartmann (1973) analyzed the Martian cratering rate relative to the lunar rate, based on then-available asteroid statistics and scaling relations, and estimated a Martian rate 6 times the lunar rate, for craters of multi-km size, with an endnote suggesting that new work might reduce this by a factor of 2 or 3 and increase the estimated ages. Hartmann (1977) more explicitly defined a parameter R_{crater} = ratio of impact crater production/km^2 -y on Mars relative to the Moon, estimating that it was around 2 for the multi-km craters that were known at that time. (This R_{crater} concept was less sophisticated than thinking in terms of R_{bolide}, because scaling relations produce a size dependence in the apparent ratio of crater production at fixed crater size D. However, this approach had some validity in the 1970s when it could be applied only to a limited D range that could be represented by one power law, as will be understood in a moment.) The Basaltic Volcanism Study Project cratering team also adopted the R_{crater} ratio and estimated that it lay in the range 1 to 4, with a best value of 2 (Hartmann et al., 1981).

These approaches yielded somewhat controversial ages of a few hundred Ma for late Amazonian geological units such as Tharsis volcanics, as early as the 1970s. The results began to look much more believable within about a year of the Basaltic Volcanism Study Project, with early recognition of Martian meteorites with ages of 1300 Ma (Wood and Ashwal, 1981; Nakamura et al., 1982; Bogard and Johnson, 1983). Wide acceptance of these as Martian igneous rock samples, however, and the acceptance that they constrained Martian chronologies, did not come for some years after that.

Starting with early Mars Global Surveyor image analysis, Hartmann (1999) reexamined the entire crater dating technique. He compared his power-law fit to the Neukum/Ivanov (1994) polynomial fit to the production function shape (log N vs. log D) and concluded that, at a first order level, the two fits were reasonably consistent with each other. The 1999 iteration adopted an "R" ratio of Mars/moon cratering of "1.6, with an uncertainty of plus a factor of 2 or minus a factor of 3," but ignored the effective D-dependence introduced by gravity and velocity scaling (see below).

As part of a larger Martian chronological study project (Kallenbach et al., 2001), Hartmann and Neukum [2001] collaborated to synthesize their systems, deriving new isochrons. This was done in collaboration with Ivanov (2001), whose data refined the R_{bolide} ratio. Hartmann and Neukum curves were derived separately, to indicate the range of uncertainty inherent in the system. Hartmann and Neukum jointly placed the Amazonian/Hesperian boundary at 2.9 to 3.3 Ga ago (but with lower probability all the way from 2.0 to 3.4 Ga ago), and the Hesperian/Noachian boundary was better fixed (being constrained by high crater densities to the late stages of decline in early cratering) at 3.5 to 3.7 Ga ago. Significantly, they proposed the Late Amazonian Epoch began 300 to 600 Ma ago, constraining late Amazonian geologic features probably to the last 13% of geologic time.

Hartmann et al. (2001) attempted a synthesis of the Neukum and Hartmann systems by using a logarithmic average of the Hartmann power law production function (made of power law segments) and the Neukum/Ivanov Martian polynomial to study Martian impact gardening. Berman and Hartmann (2002) slightly modified the Hartmann/Neukum isochron curves and used an R_{bolide} estimate of 2.0 and Hartmann power-law curves in a "2002 iteration" of the isochron system, which favored the curvature found by Neukum in the steep branch (see further discussion below).

Page 2>